Cryogenics 73 (2016) 68–72

Contents lists available at ScienceDirect

Cryogenics

journal homepage: www.elsevier.com/locate/cryogenics

Infield response of $(Co)_x$/CuTl-1223 nanoparticles–superconductor composites

M. Waqee-ur-Rehman, M. Mumtaz *, Irfan Qasim, K. Nadeem

Materials Research Laboratory, Department of Physics, FBAS, International Islamic University (IIU), Islamabad 44000, Pakistan

ARTICLE INFO

Article history:
Received 13 September 2015
Received in revised form 12 November 2015
Accepted 5 December 2015
Available online 11 December 2015

Keywords:
$(Co)_x$/CuTl-1223 nanoparticles–superconductor composites
Resistive transition broadening
Activation energy
Flux pinning

ABSTRACT

Infield superconducting properties of $(Cu_{0.5}Tl_{0.5})Ba_2Ca_2Cu_3O_{10-\delta}$ (CuTl-1223) superconducting phase after addition of cobalt (Co) nanoparticles were reported. Crystal structure of host CuTl-1223 phase was not affected after inclusion of Co nanoparticles. Superconducting resistive transition broadening was observed with applied magnetic field from 0 to 7 T, which was attributed to dissipation mechanism caused by thermally activated flux flow (TAFF) in the presence of small current (10 μA). Reduction in activation energy $U_o(H,T)$ showed suppression of flux pinning strength with increasing content of Co nanoparticles.

1. Introduction

Meissner state in high temperature superconductors (HTSCs) is lost under applied magnetic field having magnitude greater than lower critical field (H_{c1}) and HTSCs enter in mixed (vortex) state. Magnetic field penetrates in bulk HTSCs in mixed state ($H_{c1} \leqslant H \geqslant H_{c2}$) in the form of Abrikosov vortices having normal core surrounded by circulating supercurrent. Motion of these vortices either in the influence of Lorentz force or thermal fluctuation leads to the dissipation mechanism in superconducting matrix. The dissipation mechanism due to vortex dynamics is divided in three regimes; (i) flux flow when current density (J) > critical current density (J_c), (ii) flux creep when $J \sim J_c$, and (iii) TAFF when $J < J_c$ [1,2].

Motion of these vortices can be stopped by effective flux pinning. Although the pinning forces are greater than Lorentz force, in the presence of small current, flux dynamics is possible due to thermal fluctuation due to which flux vortices hop from one pinning center to other overcoming the energy barrier. The resistivity due to TAFF is given by Arrhenius law as;

$$\rho(T,H) = \rho_o \exp\{-U_o(T,H)/k_BT\} \quad (1)$$

where k_B is Boltzmann constant, ρ_o is the normal state resistivity which is independent of applied field, $U_o(T,H)$ is the activation energy.

In HTSCs, natural pinning centers are present in the form of grain-boundaries, defects and imperfections, which can stop vortex dynamics. But artificial pinning centers can also be incorporated in HTSCs matrix using different techniques; such as heavy ion irradiation, neutron irradiation and chemical doping [3–5]. Addition of different nanoparticles in HTSCs matrix is easy and novel technique to enhance flux pinning. The enhancement in flux pinning of Bi2223 superconductors with addition of different nanoparticles like ZrO_2, SiC, Sm_2O_3, Al_2O_3 and Cr_2O_3 was reported [6–11]. The improvement of flux pinning ability of YBCO superconductor after addition of different kinds of nanoparticles such as $BaTiO_3$, Al_2O_3, $BaZrO_3$ and $BaCeO_3$ was also reported [12–15]. The effects of addition of different nanoparticles in various superconducting families are observed to be different. The addition of Al_2O_3 nanoparticles in Bi2223 and YBCO families increased the flux pinning as mentioned above, whereas the presence of same nanoparticles suppressed the flux pinning ability of CuTl-1223 phase [16]. The enhancement in flux pinning activation energy of CuTl-1223 superconducting matrix was observed after addition of ferromagnetic $CoFe_2O_4$ nanoparticles, while the suppression in infield superconductivity of $GdBa_2Cu_3O_{7-\delta}$ superconductors was reported with addition of these nanoparticles [17,18]. The addition of carbon nanotubes (CNTs) results in reduction of flux pinning activation energy of CuTl-1223 superconducting phase [19]. It is, therefore, important to explore the effects of different nanoparticles (magnetic, conductors, insulators, etc.) on infield superconducting properties of CuTl-1223 superconducting phase due to diverse magnetoresistivity response of different HTSCs after addition of different nanostructures.

* Corresponding author. Tel.: +92 51 9019926 (Office); fax: +92 51 9210256.
E-mail address: mmumtaz75@yahoo.com (M. Mumtaz).

http://dx.doi.org/10.1016/j.cryogenics.2015.12.002
0011-2275/

In present research work, infield superconducting transport properties of $(Co)_x$/CuTl-1223 ($x = 0$, 0.25, 0.50, 0.75 and 1.00 wt.%) nanoparticles–superconductor composites have been studied. The unchanged crystal structure of CuTl-1223 phase after addition of Co nanoparticles shows the presence of these nanoparticles at inter-granular spaces. Resistive superconducting transition boarding has been observed with increase in applied magnetic field, which is attributed to vortex–antivortex pair-breaking due to TAFF. Supersession in activation energy $U_o(H,T)$ of CuTl-1223 superconducting phase with increasing contents of these Co nanoparticles shows the suppression of flux pinning strength.

2. Experimental details

$(Co)_x$/CuTl-1223 nanoparticles–superconductor composites with $x = 0$, 0.25, 0.50, 0.75 and 1.00 wt.% were synthesized using conventional two steps solid-state reaction. In first step $Cu_{0.5}Ba_2Ca_2Cu_3O_{10-\delta}$ precursor was prepared using $Ca(NO_3)_2$, $Cu_2(CN)_2$, $Ba(NO_3)_2$ compounds as starting materials. These compounds were mixed in appropriate ratios and ground for 2 h in agate mortar and pestle. The ground mixture was put in quartz boats for firing at 860 °C in pre-heated chamber furnace for 24 h. After furnace cooling to room temperature, again the firing of mixture under same conditions was carried out in ceramic boats with 1 h intermediate grinding. The mixture obtained after second firing was mixed with Co nanoparticles having average size of 50 nm with different wt.% (i.e. $x = 0$, 0.25, 0.50, 0.75 and 1.00 wt.%) and Tl_2O_3 in appropriate concentration, and ground for 1 h to get $(Co)_x$/CuTl-1223 nanoparticles–superconductor composites. The obtained material was pelletized under 3.8 tons/cm^2 pressure with the help of hydraulic press followed by sintering of these pellets (wrapped in gold capsule) at 860 °C for 10 min.

The structure and phase purity of the final material was determined by XRD (D/Max IIIC Rigaku with a Cu Kα source of wavelength 1.54056 Å). The cell parameters were determined by cell refinement computer program MDI (Jade) and compared with international center for diffraction data (ICDD) record. Infield resistivity as a function of temperature variation was measured by four probe method using commercial physical properties measurement system (PPMS) in the magnetic field range of 0–7 T and temperature range of 30–300 K. Low resistance contacts on samples (rectangular shaped) were made with silver paint.

3. Results and discussion

XRD patterns of $(Co)_x$/CuTl-1223 nanoparticles–superconductor composites with $x = 0$, 0.50 and 1.00 wt.% are shown in Fig. 1. These composites have tetragonal structure with P4/mmm symmetry. The crystal structure of CuTl-1223 superconducting matrix is not changed after addition of Co nanoparticles. This can be the indication of presence of these nanoparticles over the grain-boundaries rather than inside the unit cell of CuTl-1223 superconducting matrix. The small variation in *c*-axis length can be due to the stresses and strains produced in CuTl-1223 matrix after inclusion of these nanoparticles [20,21]. Moreover, the size of unit cell of CuTl-1223 phase is less than the size of nanoparticles, and atoms of added nanoparticles can only enter the unit cell after decomposition. Dispersion of nanoparticles over inter-granular sites of CuTl-1223 superconducting phase has been already reported [22,23].

Infield dc-resistivity versus temperature measurements of $(Co)_x$/CuTl-1223 nanoparticles–superconductor composites for $x = 0$, 0.50, and 1.00 wt.% in magnetic field range of 0–7 T are shown in Fig. 2(a–c). Decrease in $T_c(0)$ for all the samples is observed with increasing the applied magnetic field, which is caused by the energy dissipation mechanism due to dynamics of

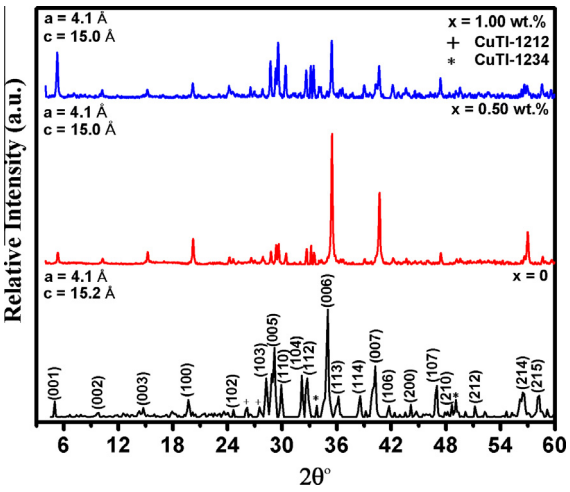

Fig. 1. XRD patterns of $(Co)_x$/CuTl-1223 nanoparticles–superconductor composites with $x = 0$, 0.5 and 1.0 wt.%.

flux vortices. Fish tail is also appeared in low temperature region [24]. The resistivity appeared in TAFF region is given by Arrhenius law given in Eq. 1. Activation energy (U_o) for TAFF is the potential barrier, which stops the hopping of flux line vortex from one pinning center to other. So to stop TAFF, it is required to increase the value of U_o, which is magnetic field and temperature dependent parameter. Arrhenius plots ($\ln(\rho/\rho_o)$ versus $1/k_BT$) of $(Co)_x$/CuTl-1223 nanoparticles–superconductor composites for $x = 0$, 0.50, and 1.00 wt.% in magnetic field range specified above are given in the insets of Fig. 2(a–c). The non-linear behavior of Arrhenius curves confirms temperature dependence of U_o along with its magnetic field dependence [25].

Field dependent activation energy $U_o(H)$ can be determined by calculating the slop of straighter part of Arrhenius curves in low resistivity region near $T_c(0)$ [26]. Plots of U_o versus applied field (H) for $(Co)_x$/CuTl-1223 nanoparticles–superconductor composites with $x = 0$, 0.25, 0.50, 0.75 and 1.00 wt.% are shown in Fig. 3. Systematic decrease in U_o with increasing content of Co nanoparticles has been observed, which shows facilitating behavior of Co nanoparticles to flux flow. This may be due to following reasons; (i) suppression in inter-grains weak-links with insertion of these nanoparticles over inter-granular sites (ii) transition of Co ferromagnetic nanoparticles to blocked state below a specific temperature, which causes reduction in potential barrier to TAFF process. Decrease in U_o with the increase in magnetic field strength is observed to obey power law (i.e. $U_o = \alpha H^{-\beta}$). The solid lines in Fig. 3 show the fitting of observed data according to the above mentioned power law. The value of β observed for $(Co)_x$/CuTl-1223 nanoparticles–superconductor composites with $x = 0$, 0.25, 0.50, 0.75 and 1.00 wt.% are 0.84, 0.75, 0.62, 0.31 and 0.46, respectively. Hence the decreasing rate of U_o with applied field is slowed down after the addition of Co nanoparticles, which can be useful for high field applications. Dependence of activation energy over different power laws in addition to above mentioned power law has been already reported in literature [27–29].

Transition width $\{\Delta T = T_c^{(\mathrm{Onset})} - T_c(0)\}$ versus applied field (H) for all the samples has been plotted in Fig. 4. The solid lines in Fig. 4 show well-fitting of transition width versus applied field to TAFF model;

$$\Delta T = \Delta T_o + \mathrm{CH}^n \tag{2}$$

where ΔT_o is transition width with no applied field and C depends upon critical current density [30]. Increase in transition width of